International Journal of Engineering Research & Technology (IJERT)
ISSN: 2278-0181
Vol. 4 Issue 05, May-2015

# Influence of Zinc on the Structural and Magnetic Properties of Copper Ferrites by Sol-Gel Auto-Combustion Method and its Antibacterial Activity

K. Anitha Rani[1] and V. Senthil Kumar[1]
[1]Department of Physics, Karpagam University,
Coimbatore-641021,
Tamil Nadu, India.

***Abstract*— Single phase spinel ferrite samples of $Cu_{1-x}Zn_xFe_2O_4$ ($0 \leq x \leq 0.5$) were synthesized by using sol-gel auto-combustion method and annealed at 1000 °C for 5 h. The prepared samples were characterized by using Thermogravimetric Analysis (TGA), X-ray Diffraction (XRD), Fourier Transform Infra-Red Spectroscopy (FTIR), Scanning Electron Microscopy (SEM), Vibrating Sample Magnetometer (VSM) and its antibacterial activity. XRD results confirm the presence of single phase spinel cubic structure in all prepared samples with crystallite size varying from 61 nm – 64 nm. No impurity peaks or phase transformation were observed in any of the samples. The vibrational frequencies of two main absorption bands of all samples are discussed from the results of the FTIR analysis. Hysteresis loops of all samples are obtained by VSM analysis. The saturation magnetization showed an increasing trend with increasing Zn content, due to the redistribution of cations at octahedral and tetrahedral sites. A comparison results for all the four samples shows that gram negative bacteria have maximum inhibition than gram positive bacteria.**

***Keywords*— Spinel ferrite; XRD; magnetic properties; antibacterial activity.***

## I. INTRODUCTION

Since 19th century, there is a rapidly growing interest in the systematic study on the relationship between chemical composition and magnetic properties of various ferrites [1]. Moreover, magnetic nanoparticles are one of the most promising materials since they possess exceptional antibacterial properties because of their large surface area to volume ratio, which is of enthusiasm to researchers due to the developing microbial resistance against antibiotics, and the improvement of resistant strains [2 - 4]. Among these, soft ferrite is one of the interesting materials, because of its magnetic, electrical and biological properties, as well as good thermal stability. It is found to be used on large scale in electronic applications, as an inductor or transformer cores, and as memory storage in CD, laptops, cell phones, etc [5 - 8]. These soft magnetic ferrites are having spinel lattice cubic structure, a mixed metal oxide with a structural formula $(A^{2+})(B^{3+})_2(O^{2-})_4$, where A and B denote tetrahedral and octahedral sites [9]. Here, $A^{2+}$ represents metallic cations like Mn, Co, Ni, Cu, Zn, Mg, and for $B^{3+}$ Fe or Al. The unit cell of spinel ferrite contains eight molecules. Each unit cell consists of 8 tetrahedral (A) sites and 4 octahedral (B) sites. The divalent cations ($A^{2+}$) occupy only A sites, it is a normal spinel structure whereas when it occupies B sites, it is an inverse spinel structure [10]. When it occupies both these sites randomly, it is mixed spinel. Among these spinels, copper ferrite ($CuFe_2O_4$) is an inverse spinel ferrite, crystallizing either in a tetragonal or cubic structure [11 - 13]. Formation of both the structures mainly depends upon the cation distribution, annealing, quenching and slow-cooling treatment [14 & 15]. Over few decades, researchers infer that by substitution of various non-magnetic ions and transition metal ions in spinel ferrites leads to improvement of their crystalline structure, magnetic properties and antibacterial activity [16 - 18].

Hence, interesting results were obtained by several methods for synthesizing nanosized magnetic spinel ferrite nanoparticles and to find its influence of dopant in magnetic and antibacterial properties, such as solid-state reaction [19], co-precipitation [20], hydrothermal [21], ceramic process [22] and sol-gel auto-combustion methods [23]. Among these methods, we have chosen sol-gel auto-combustion method, due to the fact that, with this method, significantly large amount of products can be produced within a short time. Moreover, this method is potentially suitable for manufacturing industries for preparing magnetic nanoparticles. As pointed out above, very few works have been found in literature on the zinc doped copper ferrite system and its antibacterial activity. Herein, we report the influence of doping on both magnetic and antibacterial properties of copper-zinc ferrite nanoparticles prepared by sol-gel auto-combustion method.

## II. EXPERIMENTAL PROCEDURE

Without further purification, the following chemicals were used for the preparation of nanocrystalline $Cu_{1-x}Zn_xFe_2O_4$ ($0 \leq x \leq 0.5$), by sol-gel auto-combustion method. Using a magnetic agitator, stoichiometric amounts of copper nitrate, zinc nitrate and iron nitrate were dissolved separately in double distilled water, in required molar ratios. The preparation was started by adding all nitrates with a gap of half an hour, at 50 °C. The xerogel occurred after adding

chelating agent of citric acid to nitrates is 1:1. It also acts as a fuel for self-burning combustion reaction. To get a neutralized solution of pH=7, ammonia was added drop by drop in a xerogel. The formation of aerogel occurs when the temperature is increased to 80 $^{o}$C. The complex agent of metal nitrates and citric acid was stirred continuously to get a dried gel. The dried gel was transferred into a china dish and kept in a hot plate at 100 $^{o}$C, where a voluminous tree like structure of loose ash powder was formed. The as-synthesized ferrite powder was kept in an oven at 200 $^{o}$C, overnight. The dried powder was annealed at 1000 $^{o}$C for 5 h. The final products of nanocrystalline $Cu_{1-x}Zn_xFe_2O_4$ ($0 \leq x \leq 0.5$), were characterized by TGA, XRD, FTIR, VSM and its antibacterial activity, respectively.

## III. RESULTS AND DISCUSSION

### A. THERMOGRAVIMETRIC ANALYSIS

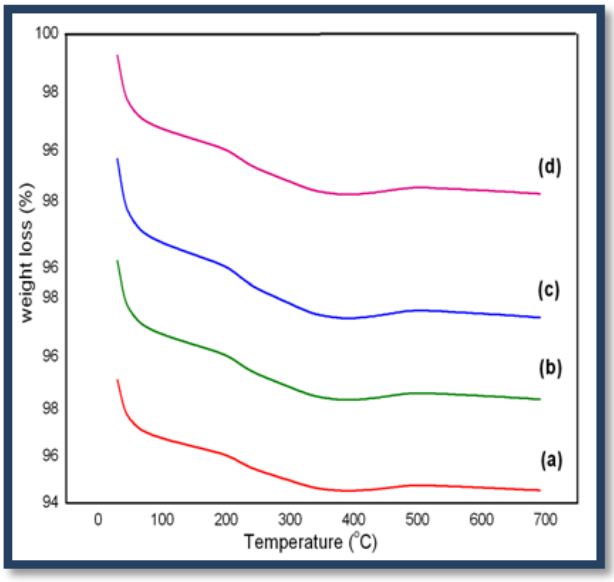


Fig. 1 TGA plots for (a) $CuFe_2O_4$ (b) $Cu_{0.9}Zn_{0.1}Fe_2O_4$ (c) $Cu_{0.7}Zn_{0.3}Fe_2O_4$ (d) $Cu_{0.5}Zn_{0.5}Fe_2O_4$ as-prepared powders

Fig.1 shows the typical TGA curves (from room temperature to 700 $^{o}$C) of as-prepared powders of all the samples of $Cu_{1-x}Zn_xFe_2O_4$ ($0 \leq x \leq 0.5$). TGA curves investigate the thermal decomposition and dehydration of the organic compounds in three different steps. In the first step, dehydration of water (hydroxyl groups) occurred at 50 $^{o}$C to 110 $^{o}$C. In second step, transformation occurred at 210 $^{o}$C to 350 $^{o}$C, which is attributed to the thermal decomposition of all nitrates ($NO_3^-$) and carboxyl groups (-COOH), respectively. Finally, above 500 $^{o}$C, the crystalline nature of all ferrite samples was observed. Hence, after 500 $^{o}$C no weight loss was noticed, which confirms the formation of ferrites. The results are shown in Fig. 1, where it can be seen that all the samples show same nature. This is because of the very low molar concentration of the dopants. Therefore, after the confirmation of crystalline nature, we have chosen 1000 $^{o}$C as a final annealing temperature for all prepared ferrite samples.

### B. X-RAY DIFFRACTION

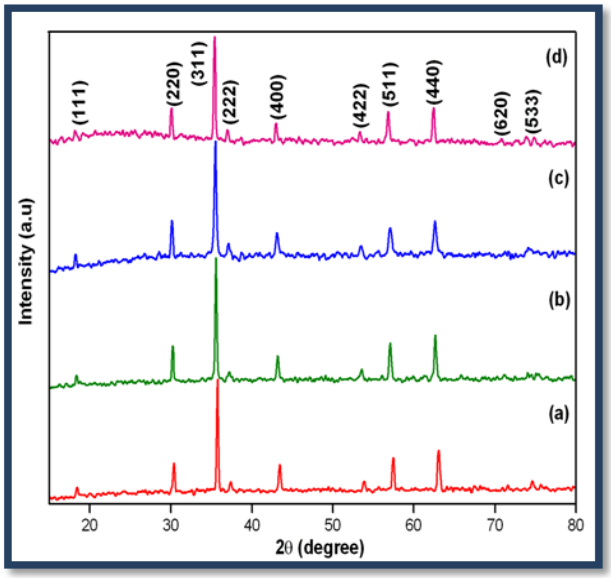


Fig. 2 X-ray diffraction patterns for (a) $CuFe_2O_4$ (b) $Cu_{0.9}Zn_{0.1}Fe_2O_4$ (c) $Cu_{0.7}Zn_{0.3}Fe_2O_4$ (d) $Cu_{0.5}Zn_{0.5}Fe_2O_4$ powders annealed at 1000 C

Fig. 2 shows the room-temperature XRD patterns of $Cu_{1-x}Zn_xFe_2O_4$ samples prepared with various Zn substitutions ($0 \leq x \leq 0.5$), annealed at 1000 $^{o}$C for 5 h. The prominent plane exists at an angle of 2θ, (111), (220), (311), (222), (400), (422), (511), (440), (620), (533), which confirmed the formation of single phase cubic spinel structures (JCPDS Card File No: 77-0010, Fd3m). No impurity peaks like $\alpha Fe_2O_3$, CuO, ZnO were observed, confirming the purity of the samples [24]. Using Debye-Scherrer formula, the particle size (D) can be calculated as, [25]

$$D = 0.9\lambda/\beta cos\theta$$

where λ is the X-ray wavelength (1.54060 Å), β is the full width at half maximum (FWHM), 0.9 is the Scherrer constant and θ is the Bragg's angle. The lattice constant ($a$) was determined by using the formula,

$$a = d_{hkl}(h^2 + k^2 + l^2)^{1/2}$$

From XRD data, the lattice constants $a$ were determined for different concentrations of Zn in $Cu_{1-x}Zn_xFe_2O_4$, and are given in Table 1, where $a$ increases from 0.839 nm to 0.842 nm with increasing Zn content. The slight increase in the values of lattice constant is attributed to the replacement of $Cu^{2+}$ (with smaller ionic radius of 0.72 Å) by $Zn^{2+}$ (with higher ionic radius of 0.74 Å) in $Cu_{1-x}Zn_xFe_2O_4$ ferrite material. This illustrates the increase of lattice constant with $Zn^{2+}$ doping, and also confirms that $Zn^{2+}$ occupies the spinel lattice. Similar variation is reported for the $Cu_{1-x}Zn_xFe_2O_4$ ferrite [22]. From Table 1, it was found that the measured density decreases from 5.48 g/cm$^3$ to 5.39 g/cm$^3$ with doping $Zn^{2+}$, and also it increases with molar concentration of $Zn^{2+}$. This may be due to the increased in unit cell volume with increase of $Zn^{2+}$ molar concentration. Hence, measured density increased.

Table:1 Structural parameters of $Cu_{1-x}Zn_xFe_2O_4$ ($0 \leq x \leq 0.5$) powder annealed at 1000 $^oC$ from XRD patterns

| Compound | D (311) (nm) | a (nm) | $a^3$ $(nm)^3$ | $\rho_{x\text{-}ray}$ $(g/cm^3)$ |
|---|---|---|---|---|
| $CuFe_2O_4$ | 61.02 | 0.834 | 0.579 | 5.48 |
| $Cu_{0.9}Zn_{0.1}Fe_2O_4$ | 37.72 | 0.839 | 0.591 | 5.39 |
| $Cu_{0.7}Zn_{0.3}Fe_2O_4$ | 59.27 | 0.840 | 0.592 | 5.40 |
| $Cu_{0.5}Zn_{0.5}Fe_2O_4$ | 63.88 | 0.842 | 0.597 | 5.41 |

### C. FOURIER TRANSFORM INFRARED SPECTROSCOPY

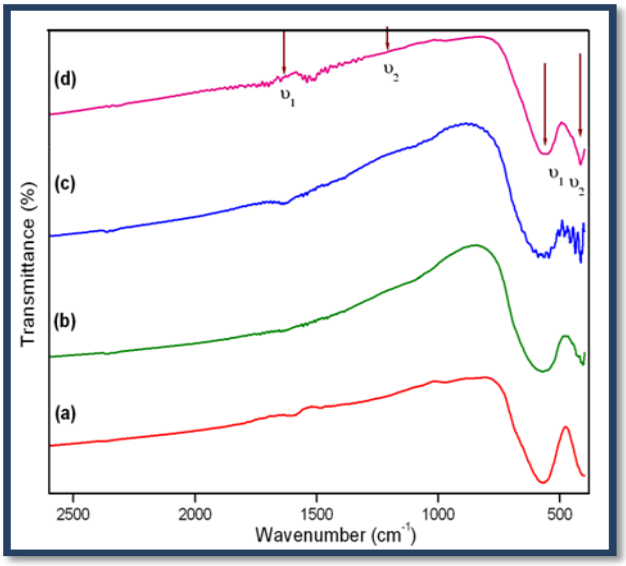


Fig. 3 FTIR spectra of (a) $CuFe_2O_4$ (b) $Cu_{0.9}Zn_{0.1}Fe_2O_4$ (c) $Cu_{0.7}Zn_{0.3}Fe_2O_4$ (d) $Cu_{0.5}Zn_{0.5}Fe_2O_4$ powders annealed at 1000$^oC$

Fig. 3 shows the FTIR spectra of the $Cu_{1-x}Zn_xFe_2O_4$ ($0 \leq x \leq 0.5$) annealed at 1000 $^oC$ in the range of 380 - 2600 $cm^{-1}$. The IR spectra show the two strong absorption bands in the range of 400 - 600 $cm^{-1}$ and two weak absorption bands in the range of 1000 - 1800 $cm^{-1}$. These two bands $\upsilon_1$ and $\upsilon_2$ belong to the intrinsic lattice vibrations of octahedral and tetrahedral sites in the spinel structure, respectively. The vibrations $\upsilon_1$ and $\upsilon_2$ of different frequency may be assigned to the long bond length of O-Me ions in the octahedral sites and shorter bond length of O-Me ions in the tetrahedral sites. Me denotes the metal ions of $Fe^{3+}$. These are most important bands are which confirm the spinel ferrite structures. From the Fig. 3, it can be confirmed that the change in band position is due to the difference in the long and short bond length distances for both the tetrahedral and octahedral complexes [26 & 27]. The bands observed at 401, 405, 416, 421 $cm^{-1}$ of $\upsilon_1$ and 567, 575, 576, 577 $cm^{-1}$ of $\upsilon_2$ in all the samples show some shift in their frequencies, due to the $Zn^{2+}$ (0.74 Å) occupying octahedral site instead of $Cu^{2+}$ (0.72 Å). Thus, it confirms the structure of mixed spinel ferrites samples. By using IR analysis, the removal of unwanted ions that can destroy a crystal lattice at that time of preparation was confirmed. Even after annealing at higher temperature of 1000 $^oC$, some absorption band peaks were observed from the range 1000 – 1800 $cm^{-1}$, which is due to traces of adsorbed $CO_2$ and O-H stretching vibrations [28].

### D. VIBRATING SAMPLE MAGNETOMETER

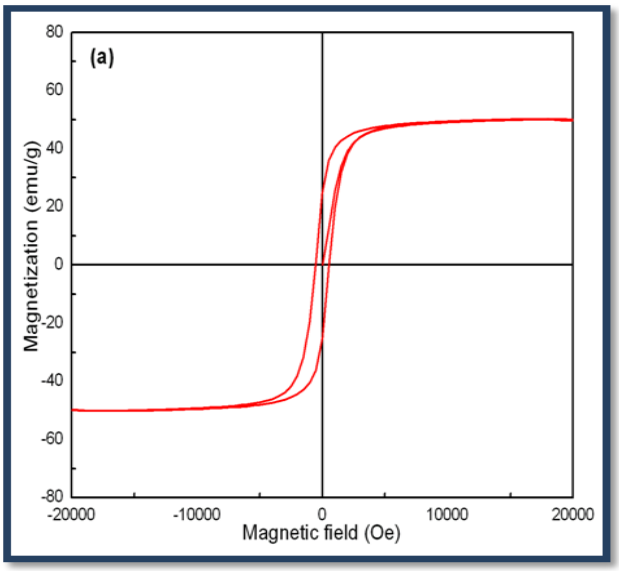


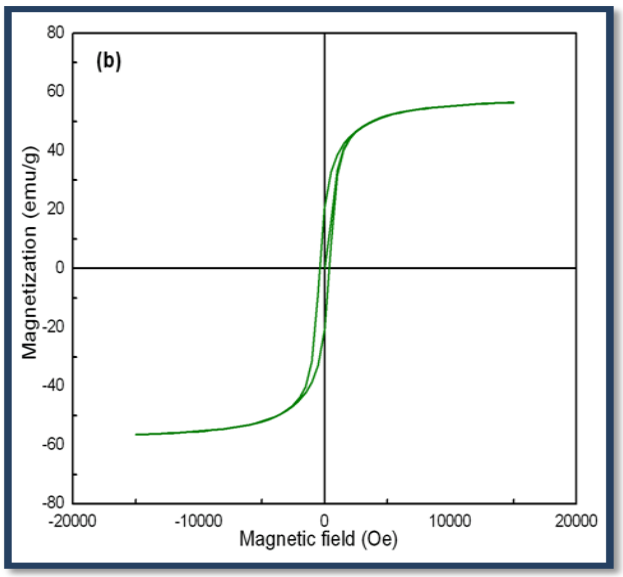

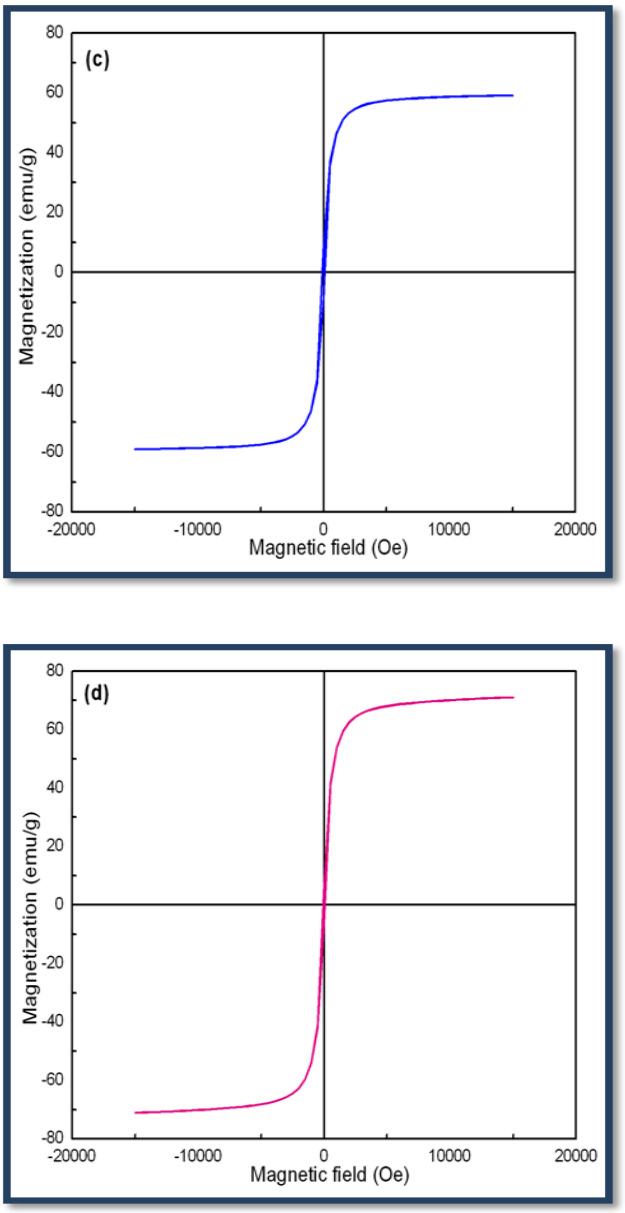


Fig. 4 Magnetization versus magnetic field behaviour of (a) $CuFe_2O_4$ (b) $Cu_{0.9}Zn_{0.1}Fe_2O_4$ (c) $Cu_{0.7}Zn_{0.3}Fe_2O_4$ (d) $Cu_{0.5}Zn_{0.5}Fe_2O_4$ powders annealed at 1000 $^oC$

Fig. 4 shows the typical room temperature magnetic properties of $Cu_{1-x}Zn_xFe_2O_4$ samples prepared with various Zn substitutions ($0 \leq x \leq 0.5$), annealed at 1000 $^oC$ for 5 h, determined by vibrating sample magnetometer (VSM) under an applied field of ±20 kOe. The values of the hysteresis measurement of coercive field ($H_c$), remanent magnetization ($M_r$) and saturation magnetization ($M_s$) of $Cu_{1-x}Zn_xFe_2O_4$ ($0 \leq x \leq 0.5$) annealed at 1000 $^oC$ are given in Table 2. From the hysteresis graph (Fig. 4b-d), the saturation magnetization is found to increase with increasing zinc content as compared to the pure samples (Fig. 4a). The increasing values of saturation magnetization are explained on the basis of grain size and interaction among the exchange in nanosize grain size particles. This leads to inter-granular magnetic correlations in a material with densely closed packed grains. It was seen in our study that coercivity decreases with increasing particle size, as reported in literature. This variation of coercivity with particle size can be explained on the basis of domain structure, anisotropy of the crystal and the critical diameter [29 - 32].

Table: 2 Magnetic properties (Coercive field ($H_c$), Remanent magnetization ($M_r$) and Saturation magnetization ($M_s$) of $Cu_{1-x}Zn_xFe_2O_4$ ($0 \leq x \leq 0.5$) annealed at 1000 $^oC$

| Compound | Hc (Oe) | Mr (emu/g) | Ms (emu/g) |
|---|---|---|---|
| $CuFe_2O_4$ | 520 | 25.1 | 50.3 |
| $Cu_{0.9}Zn_{0.1}Fe_2O_4$ | 357 | 20.3 | 56.5 |
| $Cu_{0.7}Zn_{0.3}Fe_2O_4$ | 088 | 07.6 | 59.0 |
| $Cu_{0.5}Zn_{0.5}Fe_2O_4$ | 056 | 05.1 | 71.0 |

### *E. ANTIBACTERIAL ACTIVITY*

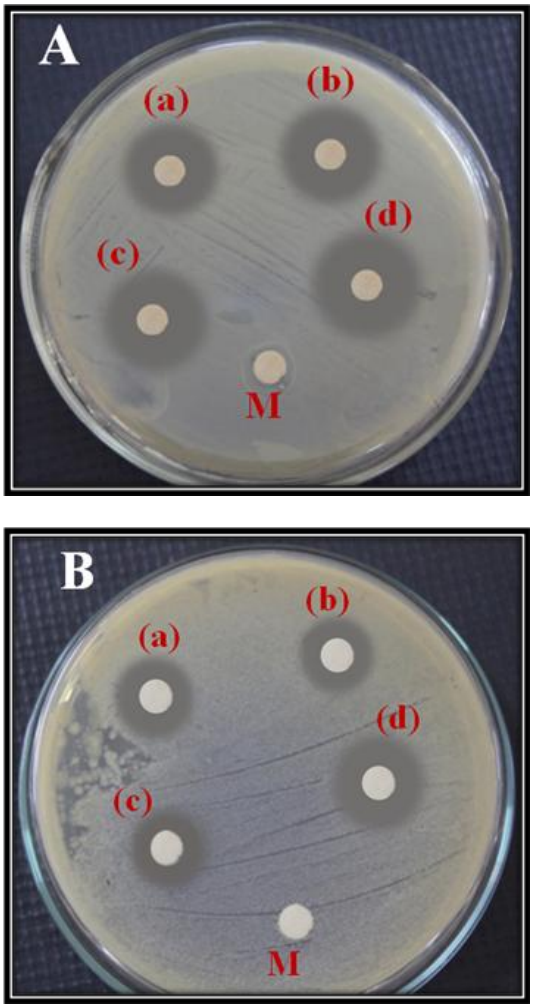


Fig. 5 Zone of inhibition of the antibacterial activity of $Cu_{1-x}Zn_xFe_2O_4$ ($0 \leq x \leq 0.5$) powders for (A) *E.coli* (gram negative) (B) *Staphylococcus aureus* (gram positive) (Note: (a) $CuFe_2O_4$ (b) $Cu_{0.9}Zn_{0.1}Fe_2O_4$ (c) $Cu_{0.7}Zn_{0.3}Fe_2O_4$ (d) $Cu_{0.5}Zn_{0.5}Fe_2O_4$ powders and M-Control)

To study the antibacterial activities of $Cu_{1-x}Zn_xFe_2O_4$ ($0 \leq x \leq 0.5$), the synthesized samples were tested against gram positive (*Staphylococcus aureus*) and gram negative (*E. coli*) bacteria, based on Kirby-Bauer disk diffusion method [33]. Fig. 5 illustrates the comparative antibacterial activities of 1mM of $Cu_{1-x}Zn_xFe_2O_4$ ($0 \leq x \leq 0.5$), which represents zone of inhibition for the growth of gram positive (*Staphylococcus aureus*) and gram negative bacteria (*E. coli*). It is well-known that the structure and the chemical composition of the cell wall are totally different for *E. coli* and *Staphylococcus aureus*. The cell wall of *E.coli*, consists of lipid A, lipopolysaccharide and peptidoglycan, whereas *Staphylococcus aureus*, mainly consists of peptidoglycan. The obtained results indicated that active oxygen species generated from transition metal oxides of pure and doped ferrites have more potential to penetrate the cell wall and decrease the cell wall division of *E.coli* instead of *Staphylococcus aureus* [35]. The comparison result for all the four samples shows that gram negative bacteria have maximum inhibition than gram positive bacteria. Furthermore, the antibacterial result shows better inhibition for doped samples than pure samples. The results reported here are better than the previous reports [34].

## IV. CONCLUSION

Influence of zinc on copper ferrite, $Cu_{1-x}Zn_xFe_2O_4$ ($0 \leq x \leq 0.5$) synthesized by sol-gel auto-combustion method confirmed that all prepared ferrite samples belongs to the single-phase spinel cubic structure with no impurities of secondary phases. TGA curves investigate the thermal decomposition and dehydration of the organic compounds in three different steps. The two vibration bands $\upsilon_1$ and $\upsilon_2$ belong to the intrinsic lattice vibrations of octahedral and tetrahedral sites in the spinel structure, respectively. From the hysteresis graph, the saturation magnetization is found to increase with increasing zinc content. Among all the four samples, gram negative bacteria have maximum inhibition than gram positive bacteria. The antibacterial result shows better inhibition for doped samples than pure samples, hence pure and doped samples have high potential to be used in memory storages, biomedical and biotechnology applications.

## REFERENCES

[1] J. A. Gomes, M. H. Sousa, G. J. da Silva, F .A. Tourinho, J. Mestnik-Filho, R. Itri, G. de M. Azevedo, J. Depeyrot, J. Magn. Magn. Mater, 300, e213-216, 2006.
[2] Mohd. Hasim, Alimuddin, Sagar E. Shirsath, S. S. Meena, R. K. Kotnala, Ameena Parveen, Aashis S. Roy, Shalendra Kumar, Pramod Bhatt and Ravi Kumar, J. Magn. Magn Mater, 341, 148-157, 2013.
[3] A. Parveen, A. R. Koppalkar, S. D. Patil and A. S. Roy, Ionics, 19, 191, 2013.
[4] Seema Joshi, Manoj Kumar, Sandeep Chhoker, Geetika Srivastava, Mukesh Jewariya and V. N. Singh, J. Molecular Structure, 1076, 55-62, 2014.
[5] Alex Goldman, Modern Ferrite Technology, second ed, Springer, New York, 2006.
[6] Sagar E, Shirsath, R. H. Kadam, A. S. Gaikwad, A. Ghasemi and A. Morisako, J. Magn. Magn. Mater, 323, 222, 2011.
[7] T. Matsunaga, R. Tomoda, T. Nakajima and T. Komine, Applied and Environmental Microbiology, 54, 1330, 1988.
[8] Lin Lin, Haiying Cui, Guanghong Zeng, Mengulin Chen, Haifang Zhang, Mingqiang Xu, Xiangqian Shen, Christian Bortolini and Mingdong Dong, 1, 2719-2723, 2013.
[9] Najmeh Najmoddin, Ali Beitollahi, Eamonn Devlin, Huseyin Kavas, Seyed Majid Mohseni, John Akerman, Dimitris Niarchos, Hamidreza Rezaie and Mamoun Muhammed, Microporous and Mesoporous Materials,190, 346-355, 2014.
[10] Deepa Thapa, Nilesh Kulkarni, S N Mishra, P L Paulose and Pushan Ayyub, Journal of Physics D: Applied Physics, 43, 1-5, 2010.
[11] S. Krupicka, P. Novak, in: E. P. Wohlfarth (Ed), Oxide Spinels-Ferromagnetic Materials, vol. 3, North-Holland, Amsterdam, 1982.
[12] G. F. Goya and H. R. Rechenberg, J. Appl. Phy, 84, 1101-1108, 1998.
[13] G. F. Goya and H. R. Rechenberg, Nanostruct, Mater. 10, 1001, 1998.
[14] J. Z. Jiang, G. F. Goya and H. R. Rechenberg, J. Phys. Condens. Mater. 11, 4063, 1999.
[15] S. C. Schaefer, G. L. Hundley, F. E. Block, R. A. McCune and R. V. Mrazek, Matell Trans. A 1, 2557, 1970.
[16] S. Guner, S. Esir, A. Baykal, A. Demir and Y. Bakis, Superlattices and Microstructures, 74, 184-197, 2014.
[17] Shanwen Tao, Feng Gao, Xingqui Liu and Ole Toft Sorensen, Mater Sci and Eng B, B 77, 172-176, 2000.
[18] N. M. Deraza and M. M. Hessain, J. Alloys. Compd, 475, 832-839, 2009.
[19] M. M. Hessin, M. M. Rashad, K. E. L. Barauy and I. A. Ibrahim, J. Magn. Magn. Mater, 320, 1615-1621, 2008.
[20] C. Venkataraju, G. Sathish Kumar and K. Sivakumar, J. Alloys Compd, 498, 203-206, 2010.
[21] H. Bayrakdar, O. Yalcin, S. Vural and K. Esmer, J. Magn. Magn. Mater, 343, 86-91, 2013.
[22] S. S. Ata-Allah and M. Yehia, Physica B, 404, 2382-2388, 2009.
[23] E. Ranjith Kumar, R. Jayaprakash, G. Sarala Devi and P. Siva Prasada Reddy, J. Magn. Magn. Mater, 355, 87-92, 2014.
[24] A. Manikandan, J. Judith Vijaya, L. John Kennedy and M. Bououdina, J. Mol. Struc, 1035, 332-340, 2013.
[25] X. Y. Li, Y. Hou, Q. D. Zhao and L. Z. Wang, J. Colloid Interf. Sci, 358, 102-108, 2011.
[26] B. K. Labde, Madan C. Sable, N. R. Shamkwar, Mater. Lett. 57, 1651, 2003.
[27] S. A. Patil, V. C. Mahajan, A. K. Ghatage, S. D. Lotke, Mater. Chem. Phys. 57, 86, 1998.
[28] E. K. Nyutu, W. C. Conner, S. M. Auerbach, C. H. Chen, S. L. Suib, J. Phys. Chem. 112, 1407-1414, 2008.
[29] M. George, A. M. John, S. S. Nair, P. A. Joy and M. R. Anantharaman, J. Magn. Magn. Mater. 302, 190, 2006.
[30] B. D. Cullity, Introduction of Magnetic Materials. Addison-Wesley Publishing Co. Inc., MA, 1972.
[31] S. Chikazumi, Physics of Magnetism. Wiley, New York, 1959.
[32] A.C.F.M. Costa, E. Tortella, M.R. Morelli, R.H.G.A. Kiminami, J. Magn. Magn. Mater. 256, 174–182, 2003.
[33] Mohd. Hashim, Alimuddin, Sagar E. Shirsath, R. K. Kotnala, Ameena Parveen, Aashis S. Roy, Shalendra Kumar, PramodBhatt, Ravikumar, J. Magn. Magn. Mater. 341, 148–157, 2013.
[34] Noppakun Sanpo, Christopher C. Berndt and James Wang, J Appl. Phys. 112, 084333 (1-6), 2012.
[35] S. Sonia, Naidu Dhanpal Jayram, P. Suresh Kumar, D. Mangalaraj, N. Ponpandian, C. Viswanathan, Superlattices and Microstructures, 66, 1-9, 2014.